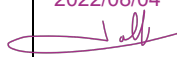


Robust quantitative in situ estimation of seismic attenuation



AUTHORS		REVIEW		APPROVAL	
Name	Date	Name	Date	Name	Date
<i>Maher Nasr</i> <i>Bernard Giroux</i> <i>Gabriel Fabien-Ouellet</i>	2021/10/04	<i>Alain Pecker</i> <i>Pierre Labbé</i>	YYYY/MM/DD 2022/08/04 	 <i>Emmanuel Viallet</i> Public access <input checked="" type="radio"/> SIGMA-2 restricted <input type="radio"/>	2023-02-17

Document history

DATE	VERSION	COMMENTS
2021/10/04	0	
2022/01/31	1	

Executive summary

We propose in this report a workflow to quantify the seismic attenuation using vertical seismic profile data acquired in shallow geotechnical boreholes. The main objective is to produce near-surface profiles for the damping coefficient or the seismic quality factor that can be integrated in the seismotectonic models build by Électricité de France (EDF) to assess the seismic hazard at the vicinity of their nuclear power plants. This processing flow is based on an innovative approach to correct geometrical spreading and on two techniques to estimate the seismic quality factor. The introduced geometrical spreading correction is performed by scaling measured amplitudes using the simulated amplitudes of an elastic wave propagating under conditions mimicking the data acquisition. Once this correction is applied, seismic attenuation may be quantified by linear regression or using a least-squares inversion. The first method assumes a layered subsurface model and relies on the fact that the amplitude reduction as function of source distances in such structures is a piecewise linear function. Fitting the segments constituting the amplitude curve permits therefore to get the attenuation coefficient of each layer. The second proposed method consists in discretizing the subsurface media using horizontal cells and defining the amplitude reduction as a linear inversion problem. This problem must be properly constrained to ensure stable solutions. A second-order Tikhonov regularization can be applied to avoid sharp fluctuation in the recovered models.

The whole workflow was tested on a synthetic dataset generated from information obtained at a real site. The results reveal that the proposed geometrical spreading correction succeeds in compensating the geometric attenuation. The same results also show that quantifying the seismic attenuation using the regression method is possible. The relative errors estimated in these examples range between 0.3 and 16%. In addition, the inversion of corrected amplitudes is able to reproduce quality factor profiles close to the true ones initially defined in the synthetic data. This supposes, however, a good choice of the implemented constrains and their corresponding Lagrange multipliers. Based on these results, future steps are essentially to test the proposed workflow on real data with different degrees of complexity.

1. Introduction

For a realistic analysis of seismic hazard, Électricité de France (EDF) is building seismotectonic models of the zones hosting their nuclear power plants. Diverse physical and geological parameters are required to build such models, for instance the subsurface structure and stratigraphy, seismic velocity models, and mechanical properties of rocks (Young and shear moduli, density....). EDF integrates the seismic attenuation in its models, and is interested in improving the robustness of *in situ* quantification of the seismic damping coefficient. This quantification should ideally take into account both small, linear elastic deformations, and larger deformations corresponding to the nonlinear domain.

The ultimate goals of the project are to map the damping coefficient variation in vertical cross-sections, allowing to locate potential seismic attenuation anomalies, and to estimate vertical profiles of the damping coefficient at borehole locations. We focus in this work on the second objective.

Available data for this project include seismic records obtained from downhole (VSP) and cross-hole surveys in geotechnical boreholes located in areas of interest, sonic log data measured with a dipole shear sonic tool, and 2D seismic reflection profiles. A preliminary study conducted by the second and third authors of this report indicates that the downhole configuration potentially allows for a more robust quantification of the attenuation than the single offset cross-hole configuration employed in previous studies performed for EDF. We thus aim here at developing an optimal processing flow to assess the seismic attenuation from Vertical Seismic Profile (VSP) data. This processing flow must account for the specificities of the surveys conducted for EDF. The first challenge addressed in this work is to properly account for geometrical spreading. Indeed, boreholes where data were recorded do not exceed 100m in depth which implies small source-receiver distances compared to the wavelength. In this case, classical geometrical spreading models used with reflection data or oil & gas VSP surveys are not applicable. Preliminary work shows that an inadequate correction leads to a significant error when determine the Q factor profile. We propose a new correction based on the ratio of measured amplitudes to elastic amplitudes obtained from full waveform modeling that correctly handles near field effects.

Once the effect of geometrical spreading is adequately removed, the corrected amplitudes are analyzed to establish a vertical profile of the P- and S-wave quality factor. Two techniques are investigated: 1- piecewise linear regression and 2- regularized least-squares method. Constraining the inverse problem is mandatory to obtain a stable solution and different approaches are investigated.

2. Methodology and theoretical background

Seismic attenuation is the physical mechanism behind the dissipation of energy during the propagation of seismic waves (Padhy and Subhadra, 2013). It manifests as a gradual decay of seismic amplitudes and the loss of the high frequency components of seismic signals as the wave propagates away from its source (Dasgupta and Clark, 1998; Reine et al., 2009). The attenuation is a function of frequency (Wang et al., 2013; Li et al., 2016). For spherical waves, three major mechanisms explain the amplitude decay. 1- Geometrical spreading: the spherical wavefront emitted by a point source expands as it propagates away from the source, leading to a reduction of energy density (Sedaghati and Pezeshk, 2016). In a homogeneous medium, the decay of the wave intensity follows an inverse-square law as function of distance from source (proportional to $1/r^2$) whereas the seismic amplitudes decrease inversely to this distance (proportional to $1/r$). 2- Intrinsic absorption (Q_i): it may be seen as the inelastic component of the seismic attenuation (Newton and Snieder, 2012). Known also as the intrinsic attenuation, absorption involves a reduction of seismic energy by internal friction of medium through which the wave travels. Elastic energy is converted into heat at the grain contacts and at the solid-fluid interfaces (Mangriotis et al., 2013). 3- Scattering attenuation (Q_{sc}): Scattering effect is mainly due to small heterogeneities present in the subsurface (Frankel and Clayton, 1986; Mangriotis et al., 2013; Sedaghati and Pezeshk, 2016). According to this mechanism, the total energy of the wavefield is

conserved and there is no real energy dissipation. However, interactions between waves and relatively small obstacles cause a random redistribution of the seismic energy in space and time (Sedaghati and Pezeshk, 2016). Scattering phenomena are manifested in seismograms by the presence of coda waves, a continuous wave train following the direct wave recording (Aki and Chouet, 1975; Frankel and Clayton, 1986). A fraction of the seismic energy is transferred to the coda and causes a relative attenuation of the first arrivals.

In real acquisitions, other possible factors may explain the variation of seismic amplitude from one receiver to another. Most notorious are the source and receiver coupling, source radiation patterns, reflection effects and wave interference (Cerveny, 2001; Giroux et al., 2001; Sedaghati and Pezeshk, 2016). These factors depend on the properties and the geometry of the subsurface medium and the acquisition system.

Seismic attenuation is usually described through a dimensionless parameter called the seismic quality factor, traditionally noted Q . It quantifies the energy loss per cycle and mainly reflect the attenuation caused by the medium (Mangriotis, 2009; Sedaghati and Pezeshk, 2016). The intrinsic attenuation and scattering effects are often combined and cannot be directly separated (Mangriotis et al., 2013; Padhy and Subhadra, 2013). In fact, the measured Q value may be considered as an effective value equal to half the harmonic mean between Q_{sc} and Q_i (Tonn, 1991). Many approaches were developed to dissociate the two factors (Padhy and Subhadra, 2013). However, a detailed description is beyond the scope of this document.

Besides laboratory measurements, quality factor is often estimated via *in situ* approaches. Several techniques were developed for this purpose and may be classified into two major categories: time domain methods and frequency-based methods. In the first class, we can mention the amplitude decay method, the risetime method and the pulse amplitude method (Tonn, 1991). In the frequency domain, notable techniques are the spectral-ratio method, the frequency shift method, the match-technique method, the spectrum-modeling method and others modified versions of previous mentioned techniques (Tonn, 1991; Quan and Harris, 1997; Mangriotis et al., 2013).

Although it is less often measured compared to other parameters, the seismic quality factor is an important property. Like other physical features, the quality factor is an intrinsic property of the medium through which waves propagate and can provide crucial information. Indeed, several emerging applications of this parameter have been recently reported in seismic reflection, vertical seismic profiling and reservoir characterization. It was proven to be a good indicator of lithology, porosity, permeability, pore fluid and saturation (Dasgupta and Clark, 1998; Mangriotis et al., 2013). Estimating a reliable Q model can be quite helpful to enhance seismic image resolution and interpretation. An accurate Q factor model is also essential to perform an Amplitude-variation-with-offset (AVO) analysis since it plays a major role to separate attenuation effects from AVO signatures (Dasgupta and Clark, 1998). The main application considered herein is earthquake engineering and in particular seismic hazard analysis and mitigation (Newton and Snieder, 2012; Padhy and Subhadra, 2013), where seismic attenuation is required to properly evaluate seismic site effects.

2.1. Geometrical spreading correction

Cerveny (2001) defined the geometric spreading (\mathcal{L}) of a spherical wave travelling between a source S and a receiver R by

$$\mathcal{L}(S, R) = \frac{1}{\sqrt{|\det(\mathbf{M})|}} \quad (1)$$

where \mathbf{M} is the matrix of second derivative of traveltime T with respect to source and receiver coordinates (Ursin and Hokstad, 2003). In 2D space, \mathbf{M} is given by

$$\mathbf{M} = \begin{pmatrix} \frac{\partial^2 T}{\partial x_S \partial x_R} & \frac{\partial^2 T}{\partial x_S \partial y_R} \\ \frac{\partial^2 T}{\partial y_S \partial x_R} & \frac{\partial^2 T}{\partial y_S \partial y_R} \end{pmatrix}, \quad (2)$$

where x_S, y_S, x_R and y_S are respectively the coordinates of the source S and the receiver R.

For homogeneous and isotropic media, the correction of the geometrical spreading attenuation consists in considering an amplitude reduction of type $1/r$ (Sheriff, 2002). Another expression, widely adopted in the seismic reflection industry, describes the geometrical spreading in the case of layered domains by $1/(t v^2(t))$. More sophisticated 2D and 3D analytical expressions were also proposed by approximating equation 1 in specific media and under diverse assumptions (Cerveny, 2001; Ursin and Hokstad, 2003; Xu and Stovas, 2017).

The previous models cannot account for near-field effects, which are predominant in shallow VSPs used in geotechnical investigations. In such conditions, we propose a novel method to compensate the effect of geometrical spreading based on 3D full waveform modeling. The idea is to estimate the amplitude decay by simulating seismic waves in an elastic medium (no intrinsic attenuation) with the assumption of a known (or previously estimated) velocity model and under the conditions replicating the data acquisition. For a smooth elastic medium, the attenuation of the selected amplitudes is expected to depend only on the geometrical spreading effect. The simulated amplitudes are used then to correct the field data.

To illustrate the mathematical formulation of the proposed approach, we consider the analytical amplitude reduction approximated as following. At a distance r from the source, the measured amplitude A_m may be expressed as:

$$A_m(r) = A_m(0) \exp\left(-\int_{ray} \alpha(r) dr\right) \Omega_S \theta_R \mathcal{L}(S, R), \quad (3)$$

where $A_m(0)$ is the source amplitude, α is the attenuation coefficient (quantifying intrinsic attenuation), Ω_S and θ_R give respectively the seismic source radiation pattern and the receiver coupling approximation. For an elastic modeling under similar conditions, the amplitude A_e variation is mainly due to the geometrical spreading and the source radiation pattern.

$$A_e(r) = A_e(0) \Omega_S \mathcal{L}(S, R), \quad (4)$$

where $A_e(0)$ is the simulated source amplitude. We assume that no significant reflections or interferences occurs during the simulation. By injecting equation (4) in (3), we obtain

$$A_m(r) = A_m(0) \exp\left(-\int_{ray} \alpha(r) dr\right) \frac{A_e(r)}{A_e(0)}. \quad (5)$$

Note that equation 5 supposes a perfect receiver coupling. Scaling the measured amplitudes by the modeled ones allows to isolate the intrinsic attenuation component

$$\frac{A_m(r)}{A_e(r)} = \frac{A_m(0)}{A_e(0)} \exp\left(-\int_{ray} \alpha(r) dr\right). \quad (6)$$

For more consistent annotation, let's assume $\frac{A_m(r)}{A_e(r)} = A_c(r)$ and $\frac{A_m(0)}{A_e(0)} = A_c(0)$. By taking the natural logarithm of equation 6, we obtain:

$$-\ln(A_c(r)) = -\ln(A_c(0)) + \int_{ray} \alpha(r) dr. \quad (7)$$

In this last equation, the intrinsic attenuation component has been isolated from the geometrical spreading effects. Processed amplitude can then be used to estimate the Q factor.

To model both elastic and viscoelastic seismic propagation, we rely on the open-source software SeisCL (Fabien-Ouellet et al., 2017), which is based on a finite difference solution of the viscoelastic wave equation. Note that viscoelastic modeling is performed here to generate the synthetic data used to validate the methodology.

2.2. Q estimation by linear regression

To solve equation 7 for the attenuation coefficient, two approaches are proposed in this work. The first is based on a piecewise constant linear regression and the second relies on a linear inversion of the seismic amplitudes.

Consider a downhole acquisition in a layered medium as shown in Figure 1. We assume a small source-borehole offset as well as a homogeneous velocity values within each layer so that we can neglect refractions at layer interfaces (normal incidence). The small offset is generally respected in real acquisitions in order to avoid the impact of tube waves (Mari and Vergnault, 2021). For amplitudes measured in the first section of the borehole crossing the first layer, equation 7 may be simplified such that:

$$\begin{aligned} -\ln(A_c(r)) &= -\ln(A_c(0)) + \alpha_1 \int_{ray} dr \\ &= -\ln(A_c(0)) + \alpha_1 L_{ray} = y_0 + \alpha_1 r. \end{aligned} \quad (8)$$

Thus, for all receivers within the first layer the amplitude ratio varies linearly with a slope equals to α_1 and an intercept $y_0 = -\ln(A_c(0))$.

For layer 2, equation 7 can be written as:

$$-\ln(A_c(r)) = -\ln(A_c(0)) + \int_S^{l_{12}} \alpha(r) dr + \int_{l_{12}}^R \alpha(r) dr, \quad (9)$$

where l_{12} is the point along the ray at the interface between layers 1 and 2 (Figure 1). For small source-borehole offsets, $Sl_{12} \approx e_1$, with e_1 the thickness of the first layer.

$$\begin{aligned} -\ln(A_c(r)) &= -\ln(A_c(0)) + \alpha_1 e_1 + \alpha_2 (r - e_1) \\ &= -\ln(A_c(0)) + e_1(\alpha_1 - \alpha_2) + \alpha_2 r. \end{aligned} \quad (10)$$

This also defines a line segment with a slope of α_2 and an intercept $y_0 = -\ln\left(\frac{A_m(0)}{A_e(0)}\right) + e_1(\alpha_1 - \alpha_2)$. Equation 10 can be generalized for a subsurface medium of n layers as follows:

$$-\ln(A_c(r)) = -\ln(A_c(0)) + \sum_{i=1}^{n-1} (\alpha_i - \alpha_n) e_i + \alpha_n r. \quad (11)$$

Equation 11 still defines a piecewise linear function of slopes equal to α_i . This may be generalized to estimate the attenuation coefficients in any layered medium. A classical piecewise linear regression can be used to determine the value α_i for each layer.

Note that the amplitudes of the real and modelled sources $A_m(0)$ and $A_e(0)$ are not required to use this method. Their values influence only the intercepts of the line segments of the curve $-\ln\left(\frac{A_m(r)}{A_e(r)}\right) = f(r)$.

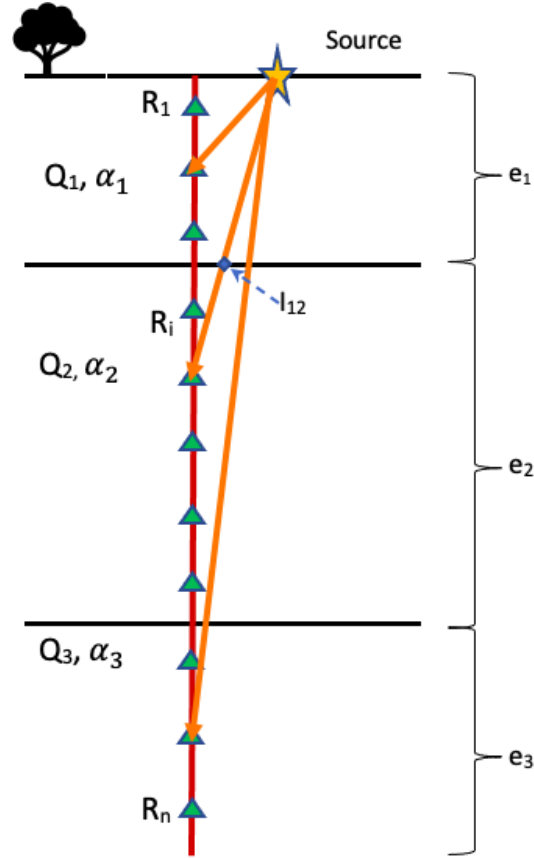


Figure 1: A simplified illustration of the downhole acquisition in layered subsurface medium. Receivers are represented by green triangles (R_1 to R_n). Three layers are assumed with different thicknesses (e_1 , e_2 , e_3) and quality factors (Q_1 , Q_2 , Q_3).

For any subsurface media, it can be demonstrated from equation 7 that:

$$\left. \frac{\partial \left(-\ln \left(\frac{A_m(r)}{A_e(r)} \right) \right)}{\partial r} \right|_{r=r_0} = \alpha(r_0). \quad (12a)$$

This means that the slope of the tangent to the curve of $-\ln\left(\frac{A_m(r)}{A_e(r)}\right) = f(r)$ is equal to the local value of the attenuation coefficient at this point. Although it is still very sensitive to noise in the data, equation 12a can be seen as a possible generalization of the regression method that permits to calculate a vertical profile for the attenuation coefficient. Using the chain rule, Equation 12a may be written in respect of depth z as:

$$\alpha(z_0) = \sqrt{1 + \left(\frac{T_x}{z_0}\right)^2} \left. \frac{\partial \left(-\ln \left(\frac{A_m(r)}{A_e(r)} \right) \right)}{\partial z} \right|_{z=z_0}, \quad (12b)$$

where T_x is horizontal source-borehole offset.

2.3. Q factor estimation by least-squares inversion

Another possible solution of equation 7 is to formulate it as an inversion problem. The first step consists in defining a discretization model of the subsurface domain. We assume a 1D model formed by M small horizontal cells with constant physical properties (velocity, density and seismic quality factor...). This allows us to substitute the integral over the seismic ray of equation 7 by a simple sum. Doing so, we get the discretized form of the amplitude reduction, written as follows:

$$-\ln(A_c(r)) = -\ln(A_c(0)) + \sum_i \alpha_i r_i \quad (13)$$

where α_i and r_i represent respectively the attenuation coefficient and the length of ray segment passing through the cell i . For data recorded at N receivers, a linear system can be defined from equation 13 as follows:

$$\mathbf{G} \mathbf{m} = \mathbf{d} \quad (14)$$

where \mathbf{G} is an N by $M+1$ sparse matrix containing ray segment lengths, \mathbf{m} is a vector of length $M+1$ containing the unknown attenuation coefficients and intercept and \mathbf{d} is the column vector of length N containing the corrected amplitudes. Explicitly, these variables are

$$\mathbf{G} = \begin{bmatrix} -1 & l_{11} & 0 & 0 & \cdots & 0 \\ -1 & l_{21} & l_{22} & 0 & \cdots & 0 \\ \vdots & \vdots & \vdots & \vdots & \cdots & 0 \\ -1 & l_{i1} & \cdots & l_{ii} & \cdots & 0 \\ \vdots & \vdots & \vdots & \vdots & \ddots & \vdots \\ -1 & l_{N1} & \cdots & l_{Ni} & \cdots & l_{NM} \end{bmatrix}, \quad (15a)$$

$$\mathbf{m} = [\ln(A_c(0)) \quad \alpha_1 \quad \alpha_2 \quad \cdots \quad \alpha_i \quad \cdots \quad \alpha_{M-1} \quad \alpha_M]^T, \quad (15b)$$

$$\mathbf{d} = - \left[\ln \left(\frac{A_m}{A_e} \right) \Big|_1 \quad \ln \left(\frac{A_m}{A_e} \right) \Big|_2 \quad \cdots \quad \ln \left(\frac{A_m}{A_e} \right) \Big|_i \quad \cdots \quad \ln \left(\frac{A_m}{A_e} \right) \Big|_{N-1} \quad \ln \left(\frac{A_m}{A_e} \right) \Big|_N \right]^T. \quad (15c)$$

Each element l_{kp} corresponds to the segment of ray k passing through the p^{th} cell (Figure 2). This element can be calculated by assuming straight seismic rays. This assumption is often respected for the receivers at depth where a normal wave incidence is predominant. At the first 10 meters from the surface, the approximation of straight seismic rays also requires a homogeneous velocity model. In the case of strong velocity variations, a raytracing step becomes necessary to take into consideration refracted waves. Note that the first element of \mathbf{m} holds the natural logarithm of the ratio between the real and modelled source amplitudes (denoted $A_c(0)$).

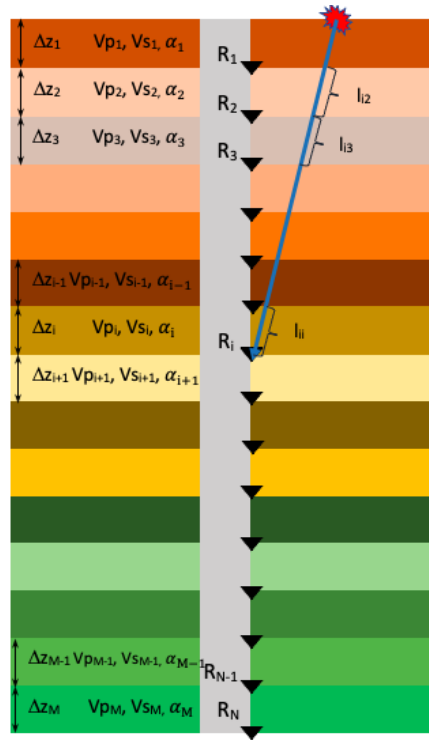


Figure 2: Domain discretization for a downhole acquisition showing source and receiver positions, parameters of each cell and an example of seismic ray path segmentation. M is taken usually greater or equal to N .

2.3.1. Regularization and Constraints

The linear system of equation 15 defines an ill-conditioned inverse problem, which should be regularized to get a stable and acceptable solution. This may be done by applying a smoothness constraint and by incorporating *a priori* information into the final solution. Here, three possible constraints are proposed:

- Regularization constraint: A second-order Tikhonov regularization is applied to avoid unrealistic fluctuations of the attenuation model. This implies the minimization of the model roughness via the second spatial derivative (Mackie and Rodi, 2010), approximated using a finite difference operator \mathbf{D} of size $M+1$ by $M+1$.

$$\mathbf{D} = \begin{bmatrix} 0 & 0 & 0 & 0 & 0 & \dots & 0 & 0 & 0 \\ 0 & -1/\Delta z & 1/\Delta z & 0 & 0 & \dots & 0 & 0 & 0 \\ 0 & 1/\Delta z^2 & -2/\Delta z^2 & 1/\Delta z^2 & 0 & \dots & 0 & 0 & 0 \\ 0 & 0 & 1/\Delta z^2 & -2/\Delta z^2 & 1/\Delta z^2 & \dots & 0 & 0 & 0 \\ \vdots & \vdots & \vdots & \vdots & \vdots & \ddots & \vdots & \vdots & \vdots \\ 0 & 0 & 0 & 0 & 0 & \dots & 1/\Delta z^2 & -2/\Delta z^2 & 1/\Delta z^2 \\ 0 & 0 & 0 & 0 & 0 & \dots & 0 & -1/\Delta z & 1/\Delta z \end{bmatrix}. \quad (16)$$

Numeric implementation of this constraint passes through the minimization of the quantity $\|\mathbf{D} \mathbf{m}\|_2^2$ in addition to the data misfit of equation 14.

- Average constraint: In the case of layered geological medium, the attenuation coefficient average value(s) of one or many layer(s) could be determined via the regression method presented in the previous section. This constraint is imposed to the final solution by minimizing an additional term equal to $\|\mathbf{H} \mathbf{m} - \mathbf{h}\|_2^2$, with matrix \mathbf{H} of size n_v by $M+1$ and \mathbf{h} of size n_v .

$$\mathbf{H} = \begin{bmatrix} 0 & \frac{1}{nc_1} & \dots & \frac{1}{nc_1} & \dots & \dots & 0 & \dots & \dots & 0 & 0 & \dots & \dots & 0 \\ 0 & \dots & 0 & \dots & 0 & \frac{1}{nc_2} & \dots & \frac{1}{nc_2} & 0 & \dots & 0 & \dots & \dots & 0 \\ \vdots & \dots & \dots & \dots & \vdots & \vdots & \vdots & \dots & \dots & \vdots & \dots & \dots & \dots & \vdots \\ 0 & \dots & \dots & 0 & \dots & \dots & 0 & \dots & 0 & \frac{1}{nc_{nv}} & \dots & \dots & \frac{1}{nc_{nv}} & 0 \end{bmatrix}, \quad (17a)$$

$$\mathbf{h} = \begin{bmatrix} \bar{\alpha}_1 \\ \bar{\alpha}_2 \\ \vdots \\ \bar{\alpha}_{nv} \end{bmatrix}. \quad (17b)$$

The parameter nv is the number of geological layers used in the linear regression. The average values of the attenuation coefficient $\bar{\alpha}_k$ are stored in the vector \mathbf{h} . The value nc_k refers to the number of cells used to discretize the k^{th} geological layer (Figure 2).

- Equality constraint: available estimates of the attenuation coefficient (or the seismic quality factor) are valuable information. Such data can be obtained from laboratory measurements or other *in situ* or indirect techniques. We can constrain the system of equation 15 to impose these values in the final solution. Consider three known attenuation coefficients $\bar{\alpha}_k$, $\bar{\alpha}_h$ and $\bar{\alpha}_l$ corresponding respectively to the k^{th} , h^{th} and l^{th} cells. We can include these values by building the following system:

$$\mathbf{F} \mathbf{m} = \begin{bmatrix} 0 & \dots & 1 & 0 & \dots & \dots & 0 & \dots & 0 \\ 0 & \dots & \dots & 0 & 1 & \dots & 0 & \dots & 0 \\ 0 & \dots & \dots & 0 & \dots & \dots & 1 & \dots & 0 \end{bmatrix} \begin{bmatrix} \ln(A_c(0)) \\ \alpha_1 \\ \vdots \\ \alpha_k \\ \vdots \\ \alpha_h \\ \vdots \\ \alpha_l \\ \vdots \\ \alpha_M \end{bmatrix} = \begin{bmatrix} \bar{\alpha}_k \\ \bar{\alpha}_h \\ \bar{\alpha}_l \end{bmatrix} = \mathbf{f} \quad (18)$$

If no laboratory measurements are available, a possible alternative is to infer some local values by fitting tangents to the curve of the function $-\ln\left(\frac{A_m(r)}{A_e(r)}\right) = f(r)$ (equation 12). Using this tangent method assumes good data quality to avoid imposing corrupted values to the inversion problem.

Considering the mentioned constraints, the final solution can be obtained with the least-squares method and written

$$\mathbf{m}^{est} = (\mathbf{G}^T \mathbf{G} + \varepsilon \mathbf{D}^T \mathbf{D} + \alpha \mathbf{H}^T \mathbf{H} + \gamma \mathbf{F}^T \mathbf{F})^{-1} (\mathbf{G}^T \mathbf{d} + \alpha \mathbf{H}^T \mathbf{h} + \gamma \mathbf{F}^T \mathbf{f}). \quad (19)$$

where ε , α and γ are Lagrange multipliers.

2.3.2. Alternative parametrizations

We may be interested sometimes to describe the seismic attenuation via the quality factor Q or other proportional quantities such as the dissipation factor ($1/Q$) or the damping coefficient ($1/(2Q)$). The first option is to invert the attenuation coefficient and then estimate Q using:

$$Q = \frac{\pi f}{\alpha V}, \quad (20)$$

where f and V are respectively the frequency and the velocity values. Numeric experiments performed to test this approach showed two undesirable effects: 1- uncertainties in the velocity model contaminate the quality factor model even if a very smooth attenuation coefficient is used. 2- variations of the Q factor model are strongly controlled by the velocity model (Figure 3). The best solution to overcome these

effects is to reparametrize the inversion problem using the seismic dissipation factor ($1/Q$). This choice is made in order to conserve the linearity of the inversion problem. Doing so, the system of equation 15 can be rewritten as follows

$$\mathbf{G} = \begin{bmatrix} -1 & l_{11}f\pi/v_1 & 0 & 0 & \dots & 0 \\ -1 & l_{21}f\pi/v_1 & l_{22}f\pi/v_2 & 0 & \dots & 0 \\ \vdots & \vdots & \vdots & \vdots & \dots & \vdots \\ -1 & l_{i1}f\pi/v_1 & \dots & l_{ii}f\pi/v_i & \dots & 0 \\ \vdots & \vdots & \vdots & \vdots & \ddots & \vdots \\ -1 & l_{N1}f\pi/v_1 & \dots & l_{Ni}f\pi/v_i & \dots & l_{NM}f\pi/v_M \end{bmatrix}, \quad (21a)$$

$$\mathbf{m} = \left[\ln(A_c(0)) \quad \frac{1}{Q_1} \quad \frac{1}{Q_2} \quad \dots \quad \frac{1}{Q_i} \quad \dots \quad \frac{1}{Q_{M-1}} \quad \frac{1}{Q_M} \right]^T. \quad (21b)$$

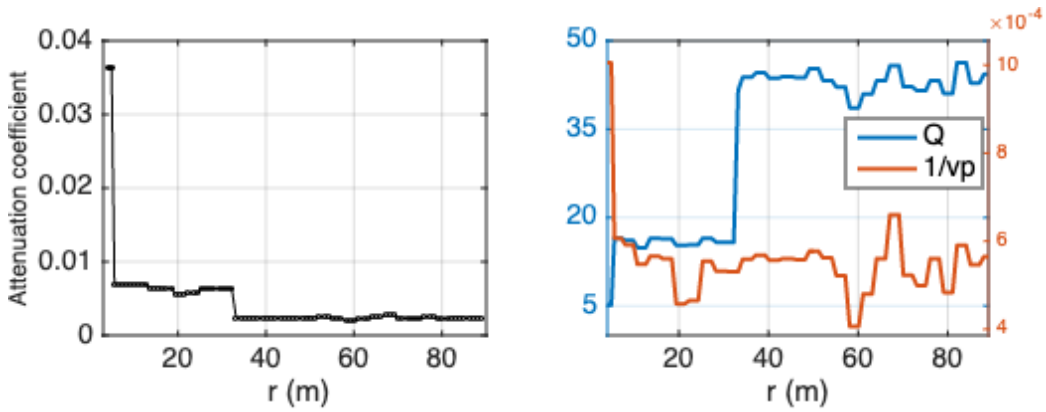


Figure 3: Velocity effects on seismic quality factor when it is determined by inverting the attenuation coefficient. Leftmost figure: determined attenuation coefficient profile. Rightmost figure: comparison between the Quality factor inferred from the attenuation coefficient profile and the slowness model (the reciprocal of velocity).

The second consideration to take into account is the reflections at layer interfaces exhibiting strong impedance contrasts, which may interfere with direct waves and affect the picked amplitudes. To deal with this issue, we add correction terms in the inversion process (sc_i terms in equation 22b). The reflection coefficient is calculated for each cell and compared to a predefined threshold. If it exceeds this threshold, corrections of the above cells are allowed by assigning a value of 1 at the appropriate entry in matrix \mathbf{G} . The system of equation 15 may be modified to hold correction terms as follows:

$$\mathbf{G} = \begin{bmatrix} -1 & l_{11} & 0 & 0 & \dots & 0 & 1 & \dots & \dots & 0 & \dots & 0 \\ -1 & l_{21} & l_{22} & 0 & \dots & 0 & \dots & 1 & 0 & \dots & 0 & 0 \\ \vdots & \vdots & \vdots & \vdots & \dots & 0 & \vdots & \dots & \vdots & \vdots & \dots & \dots \\ -1 & l_{i1} & \dots & l_{ii} & \dots & 0 & 0 & \dots & 0 & 1 & \dots & 0 \\ \vdots & \vdots & \vdots & \vdots & \ddots & 0 & \vdots & \dots & \vdots & \vdots & \dots & \dots \\ -1 & l_{N1} & \dots & l_{Ni} & \dots & l_{NM} & 0 & \dots & \dots & \dots & \dots & 1 \end{bmatrix}, \quad (22a)$$

$$\mathbf{m} = \left[\ln(A_c(0)) \quad \alpha_1 \quad \dots \quad \alpha_i \quad \dots \quad \alpha_M \quad sc_1 \quad \dots \quad sc_M \right]^T, \quad (22b)$$

where sc_i is the correction value for each cell. Note that a first-order Tikhonov regularization was applied to these corrections in order to keep their values small compared to the model parameters.

3. Results

To test the proposed approaches, a set of synthetic data was prepared. The generated examples aim at mimicking a representative downhole acquisition designed to estimate the seismic attenuation of both P and S waves.

3.1. Model parameters and data simulation

The velocity models are based on data and information taken from the “Gravelines” site. The P- and S-wave velocity models are plotted in Figure 4, and are obtained from travel time analysis of the VSP survey data. To test the attenuation algorithm, we assign a layered structure with three main horizons in which attenuations of P and S waves are constant. However, we keep the same velocity structure. Geological and physical parameters of each layer are given in Table 1. Note that the synthetic attenuation models used in these numeric tests are arbitrarily chosen and do not reflect any real scenario. The downhole acquisition realized to investigate this site includes a borehole about 90 m deep and 89 three-component geophones spaced 1 m apart. The seismic source offset is about 4 m from the borehole center. In order to reproduce real data acquisitions as faithfully as possible, two source mechanisms are considered depending on the investigated seismic phase: 1- a seismic point source with a vertical force mimicking the vertical impact of a hammer, which is usually used to maximize the impact energy in P waves (Mari and Vergnault, 2021), 2- point source with a horizontal force used to generate an SH wave in order to investigate the subsurface S wave properties (velocity and attenuation). The synthetic data are generated using a viscoelastic finite-difference-time-domain (FDTD) modeling (Figure 5), with an 8th-order Taylor spatial operator. The simulation was performed on a cubic domain with a 100 m edge and a free surface at the top. The other faces are surrounded by an absorbing CPML frame of 8 m to minimize reflections at the boundaries. To avoid numeric dispersion and ensure stability, the sampling rate and the spatial step were respectively set to 0.07 ms and 0.5 m.

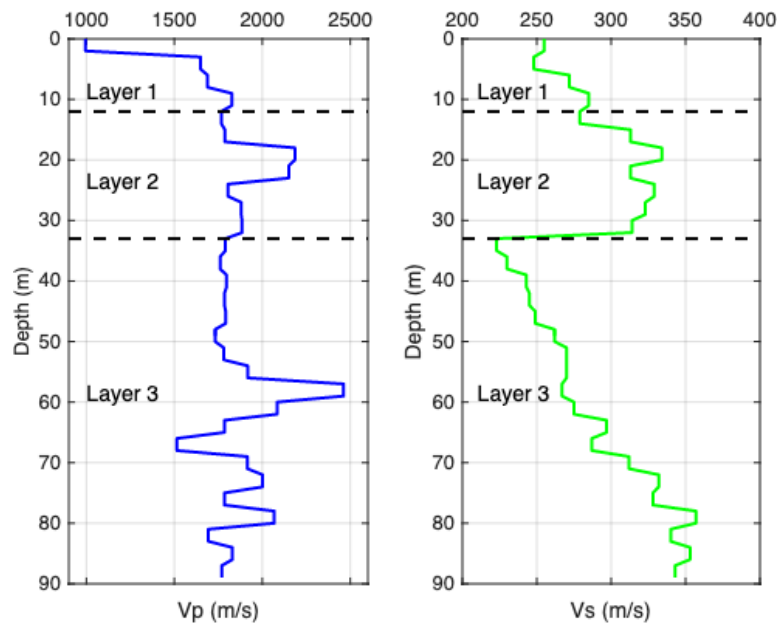


Figure 4: P and S wave velocity models.

Table 1: Layer features of the investigated site. The average velocity value of each layer was calculated using the harmonic mean.

layer	Thickness (m)	Lithology	Density	Vp mean (m/s)	Vs mean (m/s)	Model A	Model B
Layer 1	12	Sand	2.03	1454	264	$Q_1=8$	$Q_1=50$
Layer 2	21	Sandstone/siltstone	2.03	1911	314	$Q_2=20$	$Q_2=20$
Layer 3	57	Grey shale	2.00	1839	283	$Q_3=50$	$Q_3=8$

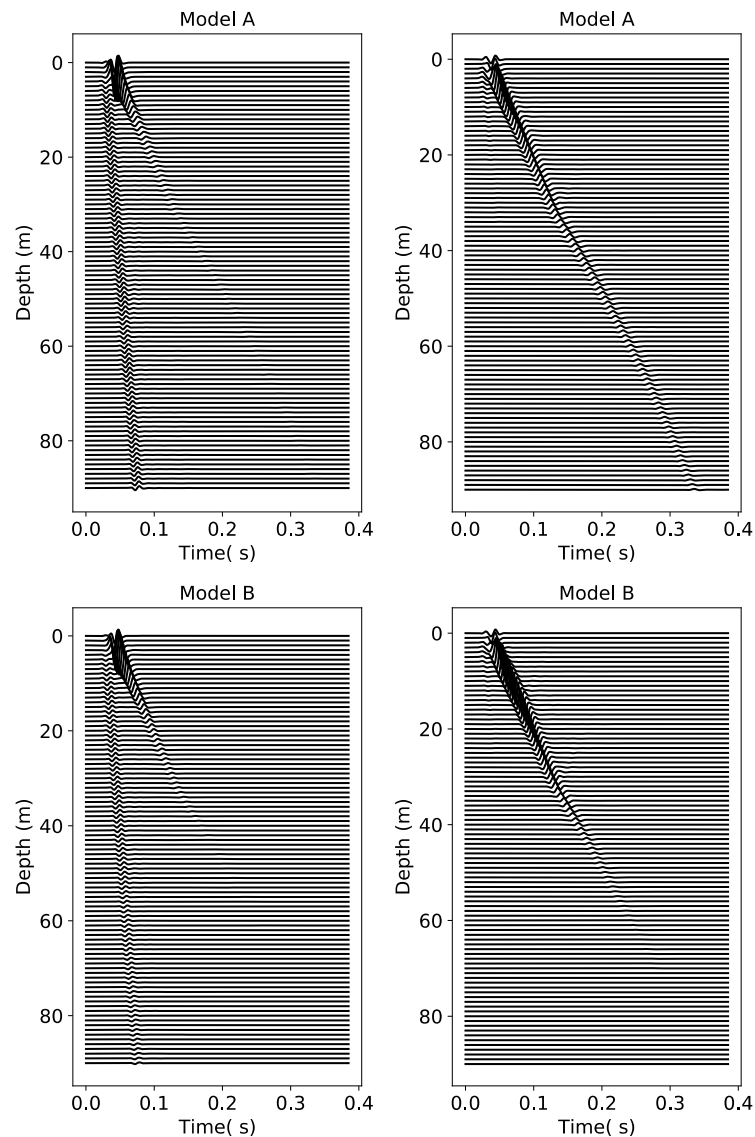


Figure 5: Synthetic datasets (Z component) prepared using Model A and B and two different source mechanisms: a vertical force for the leftmost figures and a horizontal force for the rightmost figures. A gain is applied to enhance the visibility of data in depth.

3.2. P-wave quality factor

The synthetic seismograms are used to estimate the seismic quality factors for P- and S-waves. We picked the peak-to-peak amplitudes of first arrivals with an automated algorithm. We corrected the geometrical spreading with the proposed methodology (Figure 6). We denote the corrected amplitudes A_c .

We first estimated the Q factor by the regression method (Figure 6). As expected, the curve of the inverse logarithm of corrected amplitude does show three segments that correspond to the three layers. Considering the average velocity for each layer, the seismic quality factor was calculated based on equation 20. The estimated values are given in Table 2. Note that due to the source radiation pattern and to a strong interference with S waves, P wave amplitudes for the first four receivers are too small to be reliably picked (Figure 6). These data points were simply discarded to avoid corrupting the estimation.

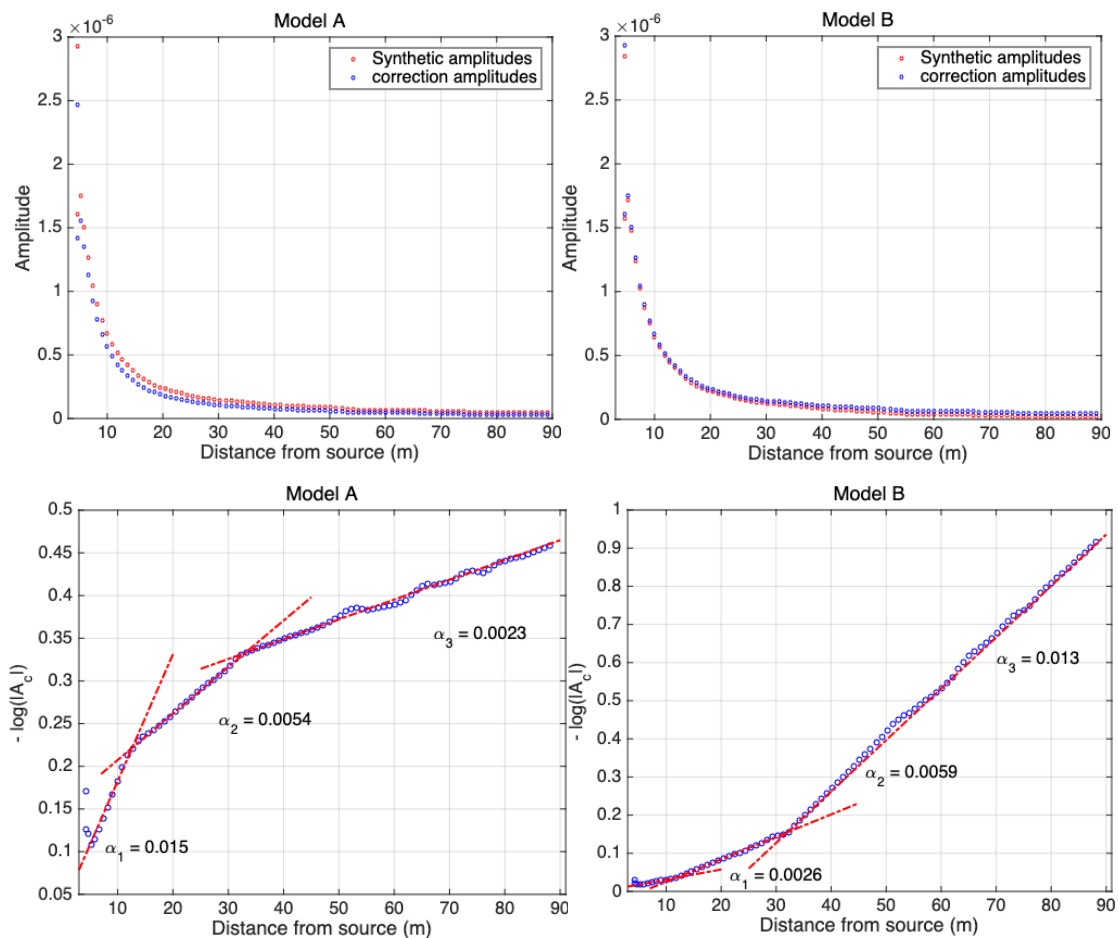


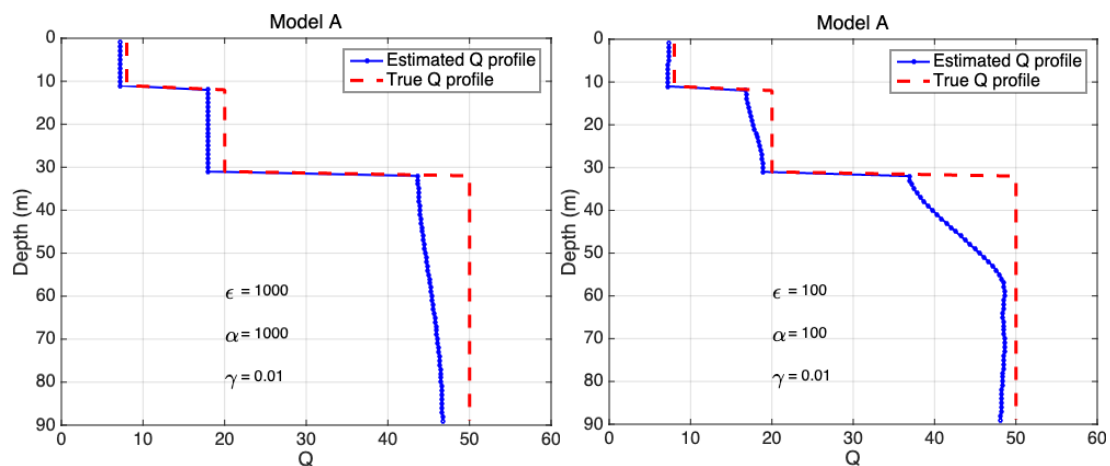
Figure 6: Picked amplitudes from the synthetic seismograms and data analysis using the regression method. Slopes of line segments that correspond to the attenuation coefficient of each layer are calculated and plotted in the bottom figures.

Table 2: Comparison between true and estimated quality factor values for Models A and B. For comparison, results obtained with amplitude data corrected using the inverse distance method are also shown.

Model		True values	Proposed approach correction			Inverse distance correction		
			Estimated values	Absolute Error	Relative Error (%)	Estimated values	Absolute Error	Relative Error (%)
Model A	Layer 1	8	8.5	- 0.5	- 5.8	4.6	3.4	42.5
	Layer 2	20	18.4	1.6	8.2	5.8	14.2	71.1
	Layer 3	50	45.4	4.6	9.2	21.4	28.6	57.1
Model B	Layer 1	50	51.6	-1.6	-3.3	9.1	40.9	81.7
	Layer 2	20	16.7	3.3	16.7	5.6	14.4	72.0
	Layer 3	8	7.6	0.4	4.6	6.4	1.6	19.7

The results obtained by regression show absolute errors between 0.1 and 5.4, which translate into relative errors ranging between 3% and 16%. Although acceptable absolute errors are obtained, relative errors appear rather high for some layers. This may be due to the use of an average velocity value for each layer as well as the low values of the true quality factors that makes small errors high when converted to relative errors. To prove the robustness of the proposed geometric spreading correction, a comparison was made with the classical spreading correction using the inverse distance from source. As expected, the proposed correction can better isolate the geometric spreading effect and guarantee more reliable estimates. Correcting the seismic amplitudes using the inverse distance generally leads to over-estimating the geometrical spreading effect and therefore under-estimating the intrinsic attenuation (Table 2).

We then applied the least-squares inversion approach. The problem was parameterized via the seismic dissipation factors (equations 21) and includes correction terms to compensate potential interference effects where strong impedance contrasts are present. The results are shown in Figure 7. Depending on the value of the Lagrange multipliers (ϵ , α and γ) the true Q factor values are relatively well reproduced. Note that in both examples, models with the highest smoothing constraint ($\epsilon = 1000$) give estimates closer to the real profiles. This may be explained by the fact that we initially used piecewise constant models so that smoother models can better reproduce them.



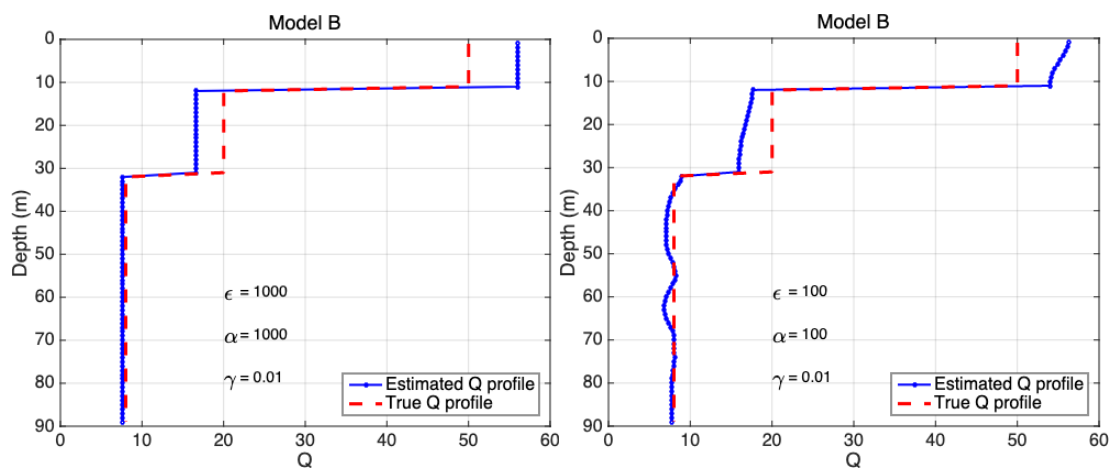
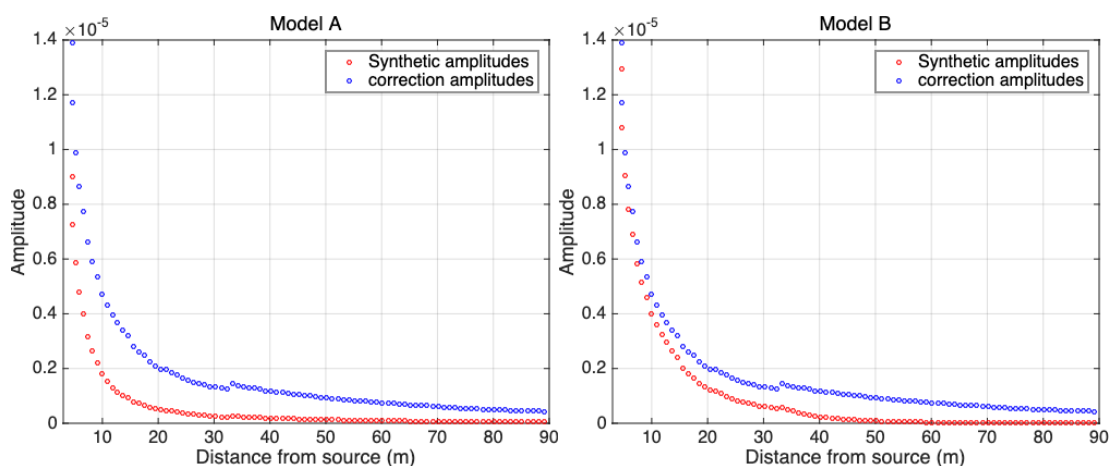


Figure 7: Seismic Quality factor profiles determined by inverting the corrected amplitudes presented in Figure 6. Different values of Lagrange multipliers (ϵ , α and γ) are used, as indicated in each subfigure.

3.3. S-wave quality factor

The same methodology was applied to analyze S-wave data. Picked amplitudes before and after geometrical spreading correction are illustrated in Figure 8. Compared to P wave data, two observations can be noted: 1- The curves of $A_m(r)$ and, especially, $A_e(r)$ show jump discontinuities at $r = 32$ m. This may be due to the strong reflection that takes place at the interface between Layer 2 and 3 caused by a sharp velocity variation ($R \approx 0.18$). The reflected waves travelling back interfere with the direct waves and could therefore affect their amplitudes. This effect is clearly noted for $A_e(r)$ since with no intrinsic attenuation the wave arriving at the mentioned interface has more energy and produces stronger reflections and interferences. 2- The curve defined by the corrected amplitudes is not perfectly linear for Layer 3, especially in the case of Model B (Figure 8). This was expected since the assumption of a constant quality factor combining with strong variation of the velocity values within this layer induce a non-constant attenuation coefficient (this can be deduced from equation 20). Indeed, the velocity of layer 3 with values ranging from 223 m/s to 350 m/s better defines a gradient model than a constant one (Figure 4).



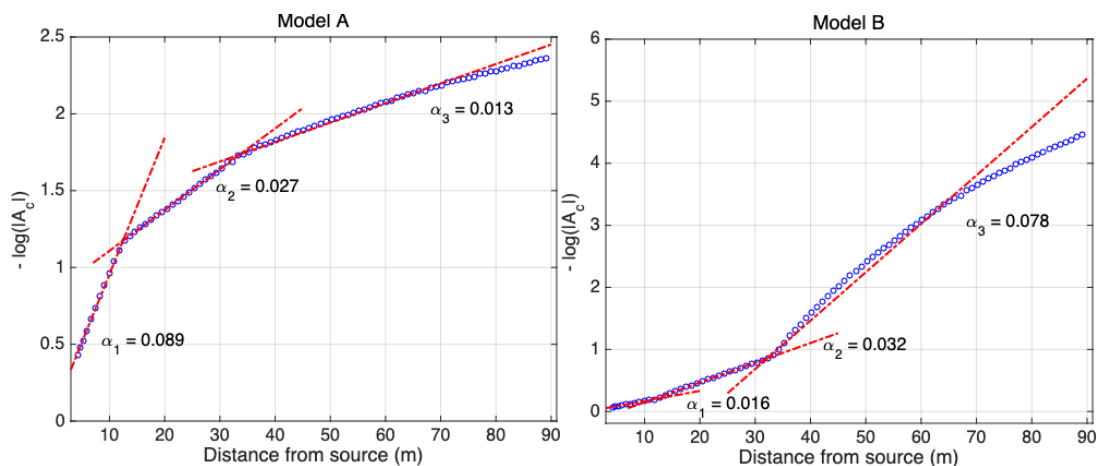


Figure 8: Picked S wave amplitudes of synthetic seismograms and analysis of the corrected amplitudes using the regression method. The attenuation coefficient determined for each layer is plotted in the bottom figures and near the correspondent line segment.

A first analysis of picked amplitudes was made using the regression method. Estimated S-wave quality factor values are presented in Table 3. Absolute and relative errors are globally lower than those obtained for P waves. A comparison with the classical inverse distance correction was also performed and yields similar results. It confirms that the proposed correction is better to compensate the geometric spreading effect. Note that for both models, the inverse distance correction shows higher errors for the layer 1 since the method is not appropriate for data collected at small distances from the source.

Inversion of the S-wave amplitudes was also performed in a second step. The inverse problem was also parameterized via the dissipation factors ($1/Q$) and used the same correction terms as for P-waves (albeit with different Lagrange multiplier values). Estimated Q factor profiles are plotted in Figure 9. The results are generally similar to those already determined for the P waves and confirm the previous observations: strong regularization constraints better reproduce the true models in this experience.

Table 3: Comparison between true and estimated S wave quality factor values for Model A and B. Results obtained by applying the introduced geometric spreading correction and the classical inverse distance correction were included.

Model		True values	Proposed approach correction			Inverse distance correction		
			Estimated values	Absolute Error	Relative Error (%)	Estimated values	Absolute Error	Relative Error (%)
Model A	Layer 1	8	8.0	0.0	0.0	3.2	4.8	60.4
	Layer 2	20	22.6	-2.6	-13.1	16.7	3.3	16.5
	Layer 3	50	52.5	-2.5	-5.0	42.2	7.8	15.6
Model B	Layer 1	50	43.5	6.5	13.0	4.7	45.3	90.7
	Layer 2	20	18.9	1.1	5.7	14.6	5.4	27.2
	Layer 3	8	8.5	-0.5	-6.7	10.0	-2.0	-25.0

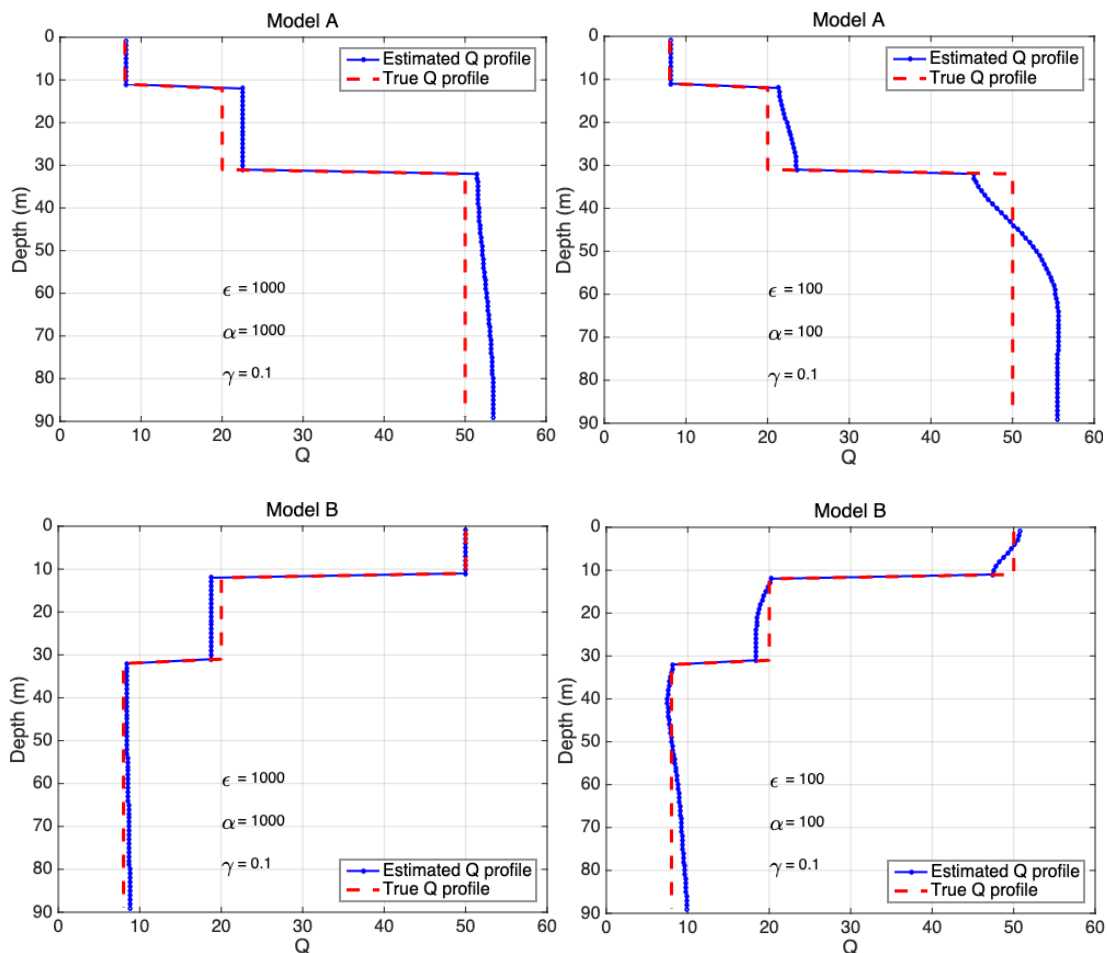


Figure 9: Seismic Quality factor profiles determined by inverting the S wave amplitudes. Different values of Lagrange multipliers are tested. Used values for each experiment are mentioned on the correspondent figure.

4. Analysis of noise and uncertainty effects

Starting from the fact that the proposed correction is based on a numerical simulation of the wavefields in an ideal elastic domain with simplified features compared to the real medium, it seems worthwhile to investigate the effect of a number of factors having strong control upon the measured amplitudes. Considering the downhole acquisitions adopted by EDF, the variables of interest include the seismic source position (uncertainty on the measured coordinates), mechanism (force orientation) and frequency, the receiver depths, coupling and horizontal axis orientations as well as the subsurface velocity and density models. The measurements or the *in-situ* estimations of all these parameters are subject to uncertainty and noise effects at different degrees. Generally, we expect that the uncertainties associated with the seismic source and receiver parameters are lower than those related to the subsurface characteristics. Thereby, we limit our error analysis to the effects of the velocity and the density models.

4.1. Velocity model effect

For a downhole acquisition, velocity models are often estimated by considering the arrival times of the direct waves. This task is subject to a non-negligible uncertainty since various error sources can impact the final estimates at different stages. This list includes for example the ambient noises contaminating

the recorded signals, the seismic phase identification, the wave interferences as well as the first break picking errors. Moreover, using an inversion process to infer the velocity models from the arrival times is known to be an ill-posed problem which implies a non-unique solution.

To quantify the effect of the velocity errors, we relied on a Monte Carlo analysis. First, we started by generating 1000 random P-and S wave velocity models. These samples are independent and follow two multivariate normal distributions with means equal to the noise-free velocity models used to generate the synthetic data of Figure 4. Furthermore, the used distributions have diagonal covariance matrices (independent elements) with standard deviations of 5%. The probability density functions (pdf) used in this experiment are plotted in Figure 10. For each sample, a full waveform modeling was then performed to estimate the correction terms ($A_e(r)$). We adopted for this stage the same simulations conditions used to prepare the synthetic data of Figure 5 such as the domain dimensions, the CPML layer, the temporal and spatial discretization steps and the seismic sources parameters.

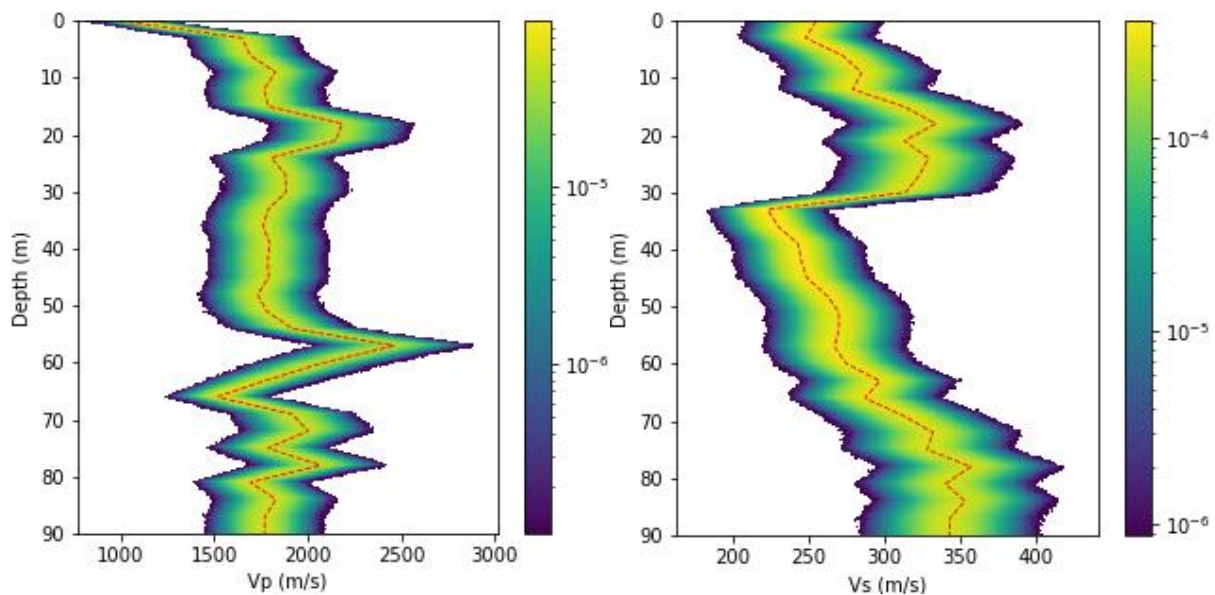


Figure 10: Velocity probability density functions of P-and S wave used to generate the random samples. Red dashed lines give the mean of each distribution.

4.1.1. Velocity effects upon geometrical spreading correction

After calculating the correction terms for each velocity model, we obtained a set of 1000 correction curves. This set is then used to generate the probability distributions associated with the correction terms of both P-and S-waves. The two pdfs are plotted as function of depth z in Figure 11. An overview of their graphs permits to note that the shapes of the determined distributions are very similar to the correction term curves obtained with noise-free data (Figure 6 and Figure 8) with almost the same variations and the jump discontinuities. One can also observe that the variances of these distributions are higher at small distances from the seismic sources (Figure 11). For example, the P wave correction distribution shows standard deviation values ranging between 1.6×10^{-7} m/s at 1 m depth and 1.9×10^{-9} m/s at 80 m depth. The S wave correction standard deviations calculated at the same depths decrease from 1.4×10^{-6} m/s to 1.8×10^{-8} m/s. This may be interpreted by the fact that seismic waves have higher amplitudes at the vicinity of sources. Considering these amplitudes as random variables, it is well expected to have higher variances for variables with larger order of magnitudes. This may also explain the observation of a higher dispersion of S-wave distribution compared to the P wave dispersion (Figure 11). Finally, the high variances near the seismic sources may be also due to a predominant effect of data noises in this zone.

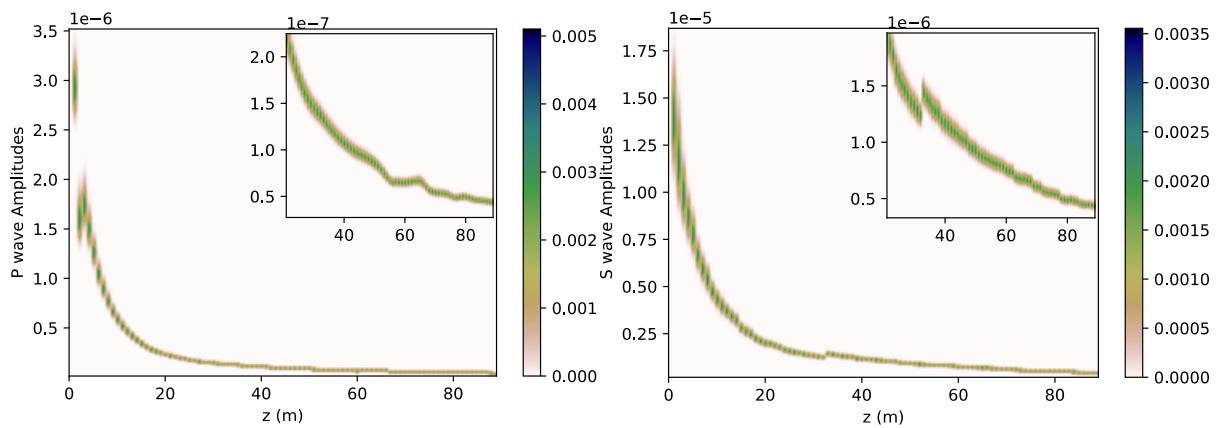
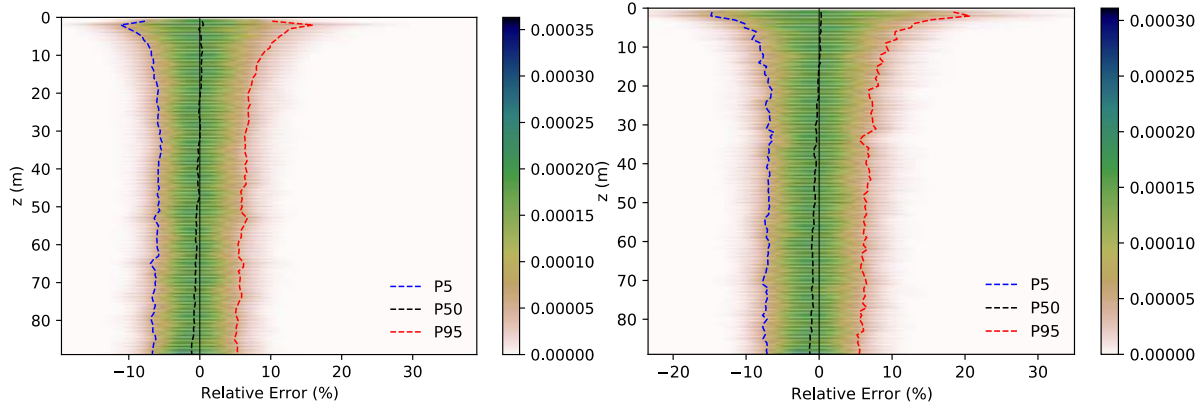


Figure 11: Probability density functions of correction terms as function of depth z for respectively P (leftmost) and S (rightmost) waves. Zooms on the graphs between $z = 21$ m and $z = 90$ m are plotted in the upper right corner.

Besides the correction term distributions, we also calculated the pdf of the relative errors (Figure 12). The correction terms calculated using the noise-free data are taken as reference values (Figure 6 and Figure 8). Plotted as function of depth, error pdfs for both P-and S-waves show similar variations. Furthermore, generated errors seem to be correlated with the distances from the source, with high values being observed near the source. Concerning the means of these distributions, we note values very close to zero (Figure 12). This implies that the white noises added to perturbate the velocity models do not introduce, on average, a bias in the correction term estimates. This was observed especially at the vicinity of sources whereas a slight negative bias is noted for the correction terms at depth (Figure 12).



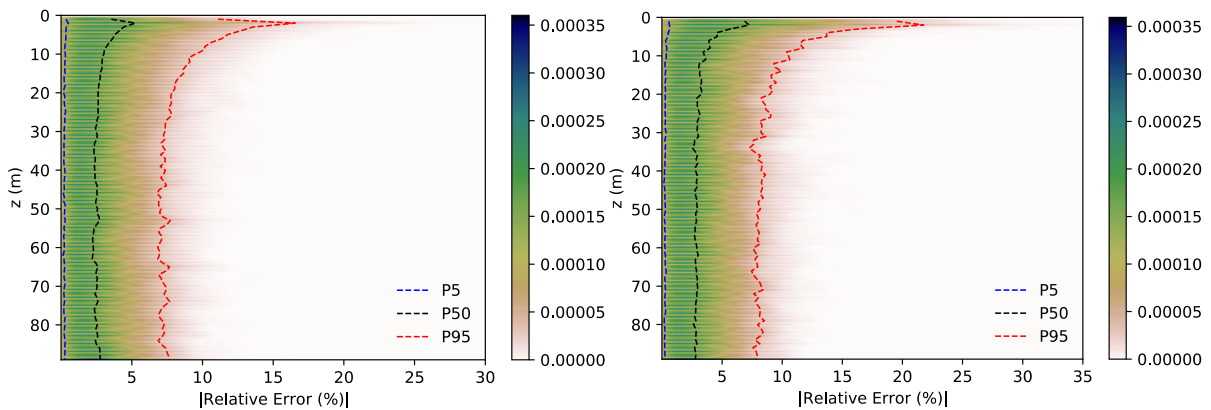


Figure 12: Relative error and its absolute value distributions for respectively P (leftmost) and S (rightmost) waves. The 5th (P5) and 95th (P95) percentiles as well as the median (P50) are calculated and plotted for each distribution.

In absolute value, the relative error distributions show slightly higher values for S-waves compared to P-waves, especially near the seismic source (Figure 12). The means of these distributions range between 6% and 3% (3.2% in average) for P waves and between 8% and 3% (3.7% in average) for S waves. Note that these values are in the same order (even less) compared to the relative error means of the contaminated velocity models using in this experiment (estimated to 4%). The added noises are not amplified in the output correction terms. This means that the proposed correction method is globally stable and does not exacerbate velocity errors in the resulting correction terms.

4.1.2. Velocity effects upon quality factor estimation

Using the correction terms calculated for each velocity model realization, the analysis was extended to investigate the robustness of the proposed methods to infer reliable Q factor estimates. The tests consist in considering the synthetic dataset of Model A (which were prepared via a viscoelastic modeling) and applying the geometrical spreading correction using the terms calculated with the 1000 velocity samples contaminated with noise (Figure 11). The two proposed methods (the linear regression method and the least-squares inversion) are then applied to estimate the Q factor values. Comparison with the true values is finally done.

- Linear regression method: The curves of the different realizations of the corrected data were linearly fitted to get the slopes of the 3 segments. The determined attenuation coefficients were then used to calculate the quality factors of the 3 layers of Model A (Table 1). Following a realistic data processing, the average velocity of each layer was estimated by considering the noisy models. The histograms of the quality factor values obtained for the P- and S-waves are respectively plotted in Figure 13 and Figure 14. Besides, the histograms of relative errors calculated with reference to the true quality factor of each layer were drawn in the same figures. Finally, the pdf corresponding to the distribution of the quality factor and associated errors were fitted for each layer (Figure 13 and Figure 14). Using the criterion of total mean squared error, a lognormal distribution was chosen for this purpose.

From the obtained results, three important observations can be made: 1- the determined quality factor estimates are slightly biased. The average values for P-waves are respectively 8.1 for Layer 1, 19.2 for Layer 2 and 50.5 for Layer 3. Similar values were obtained with the S wave data. This bias is may be due to the different approximations assumed in the linear regression method. 2- Although gaussian noise was added to perturbate the velocity models, a lognormal distribution can better fit the obtained quality factor values and the associated relative errors. 3- Quality factor estimates of S-waves seem to be more reliable than P-waves. The calculated average errors range from 16% for Layer 3 to 19% for Layer 1 and 2 in the case of P waves whereas they do not exceed 10% for S waves. Recall that the Q

factors are calculated in this experiment using the contaminated velocity values so that a non-negligible component of obtained errors correspond in fact to the velocity model perturbations. Note also that almost 5% of P wave data lead to very poor estimates (error > 100%) and were discarded from the presented results (Figure 13) for visibility reasons. The issue was not observed for S wave data. In short, the estimation of quality factors of the compression waves seems to be trickier than for the shear waves, at least for this example. We finish this analysis by recalling that the performed test does not take into consideration the human-driven data quality control of which is often made in real processing (we rely on a fully automatic procedure here).

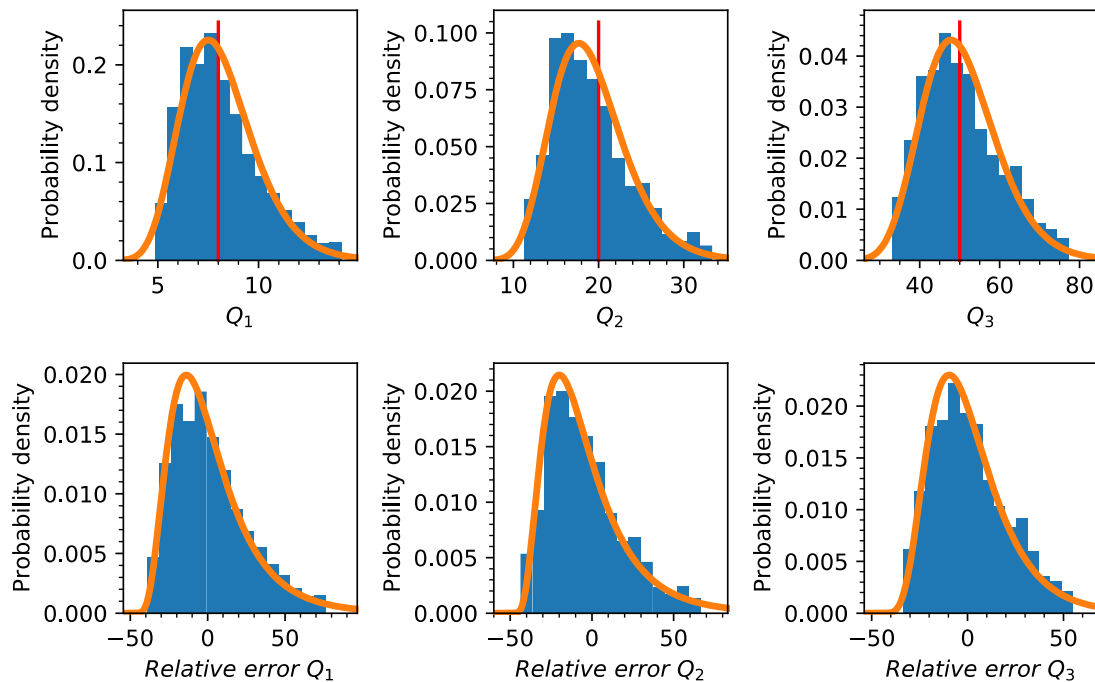


Figure 13: Probability density functions of P wave quality factors (upper 3 figures) and the associated relative errors (lower figures) for the 3 layers of Model A. Vertical red lines indicate the true quality factor of each layer.

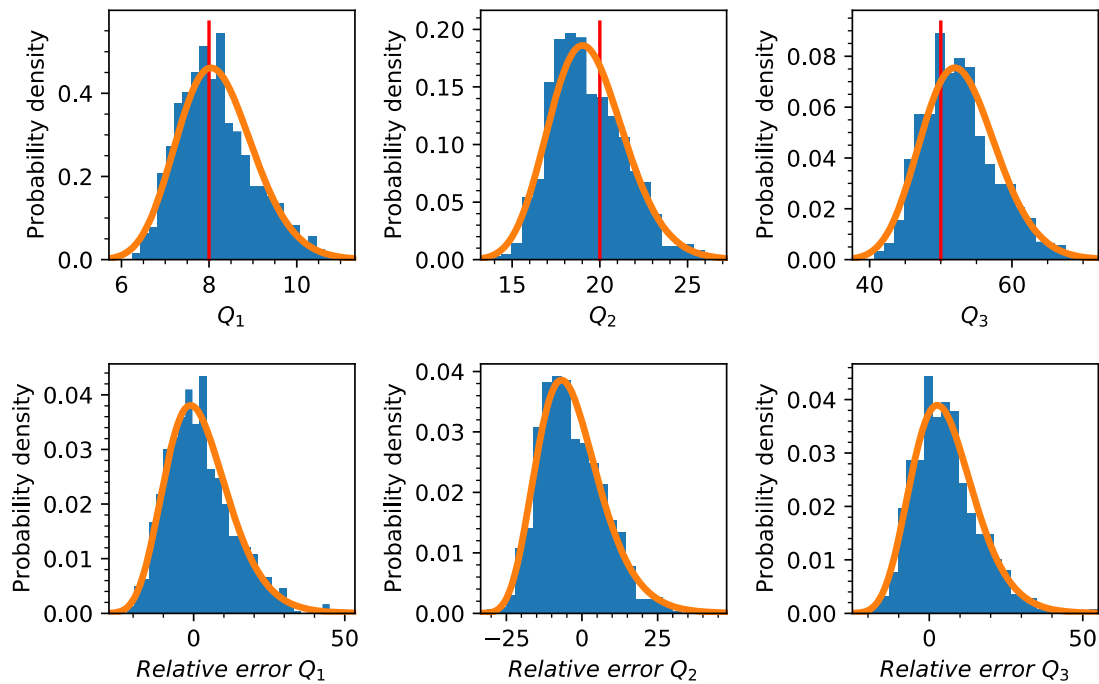


Figure 14: Probability density functions of S wave quality factors (upper 3 figures) and the associated relative errors (lower figures) for the 3 layers of Model A. Vertical red lines indicate the true quality factor of each layer.

- The least-squares inversion: The data corrected with the different terms were also tested with the inversion method. For this experiment, the Lagrange parameters were respectively fixed to $\varepsilon=1000$, $\alpha=0.01$ and $\gamma=0.01$. Inferred profiles were therefore used to generate the probability distributions of the P- and S-wave quality factors (Figure 15). The analysis of obtained results show that: 1- Both P and S wave quality factor pdfs seem to follow a 2D lognormal distribution. P wave pdf is more asymmetrical compared to S wave. Moreover, the dispersions of the two distributions are quite different with larger variance values were noted for the P wave pdf. 2- Both P- and S-wave dispersions increase with depth. It is easy to note, for example, that the Q factor pdf corresponding to Layer 3 has larger variance compared to Layer 1 (Figure 15). 3- the estimated profiles seem to be biased. The average value profiles do not match the true quality factors assumed in this test. However, they are so close to the profile obtained with the noise-free data (Figure 7 and 9). This means that the bias is not related to the added errors.

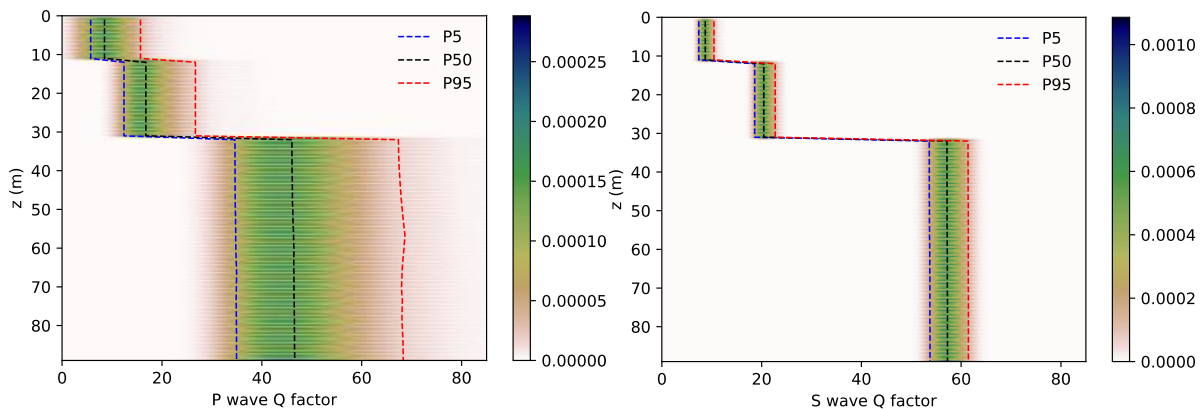


Figure 15: Probability distributions of P and S wave quality factors. The 5th (P5) and 95th (P95) percentiles and the median (P50) are calculated and plotted for each distribution.

4.2. Density uncertainty effects

Density of the various lithologies is often poorly constrained. To analyze the effects of density uncertainty upon the proposed geometrical spreading correction and the whole methodology aiming at quantifying the seismic quality factor, a series of numerical experiments using a Monte Carlo approach was also carried out. The task consists in considering again Model A and trying to contaminate its density profile by adding white noises. For this purpose, 1000 density model samples were generated using 2 independent gaussian distributions with means equal to the noise-free density model (Table 1) and standard deviations of 5% (Figure 16).

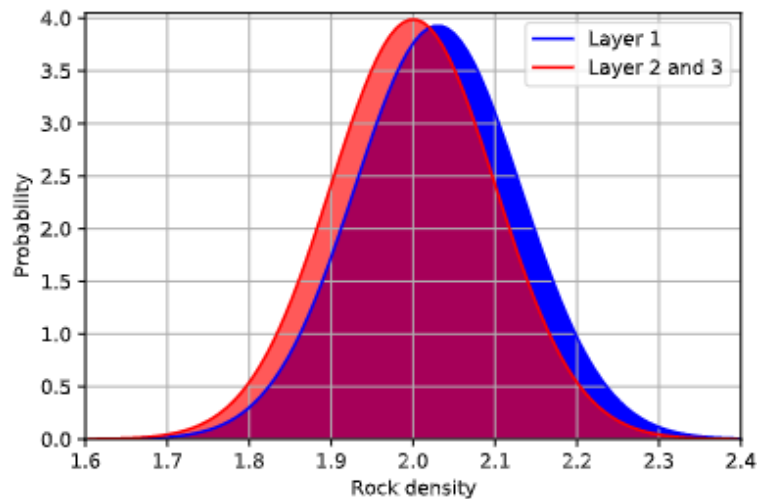


Figure 16: Rock density distributions of the 3 layers of Model A used to perform the Monte Carlo analysis.

4.2.1. Density effects upon the correction terms

For each density model, the correction terms ($A_e(r)$) were determined by picking a set of synthetic seismograms prepared using a full waveform modeling. The velocity models of P- and S-waves are kept noise-free for this experiment. The other simulation parameters are also kept invariant (CPML layer, temporal and spatial steps and seismic sources...). Obtained correction term samples permit then to generate the corresponding probability distributions (Figure 17). Compared to the previous tests, we can note that the shapes of these distributions are still very similar to the curve of the correction terms calculated using noise-free data. Unlike the pdfs obtained with the analyses of the velocity model effects, the dispersions of these distributions are lower near the seismic sources. Their standard deviations range from 4.5×10^{-10} m/s at 1 m depth to a maximum of 1.5×10^{-8} m/s at 13 m depth for P-waves and from 3.5×10^{-11} m/s to a maximum of 1.2×10^{-7} m/s for S waves at the same depths. This is further confirmed by calculating the relative errors and convert their values to probability distributions (Figure 17). The results show a strong similarity between the distributions of P and S wave errors and some differences between the induced errors of the 3 considered layers of Model A. In Layer 1, very low errors were recorded. Perturbations of the density of this layer seem with no significant effect on the proposed correction. Error distributions at the depth of Layer 3 show a zero mean value and an average error of 2.6%. Layer 2 displays typical error distributions compared to other layers: A constant positive bias is observed for the correction term estimates. Besides, slightly higher errors are noted within this layer (2.7% in average). These different behaviors may be explained by the reflections occurring at layer interfaces due to density contrasts. These reflections have a direct effect on the transmitted energy and the interference between seismic waves.

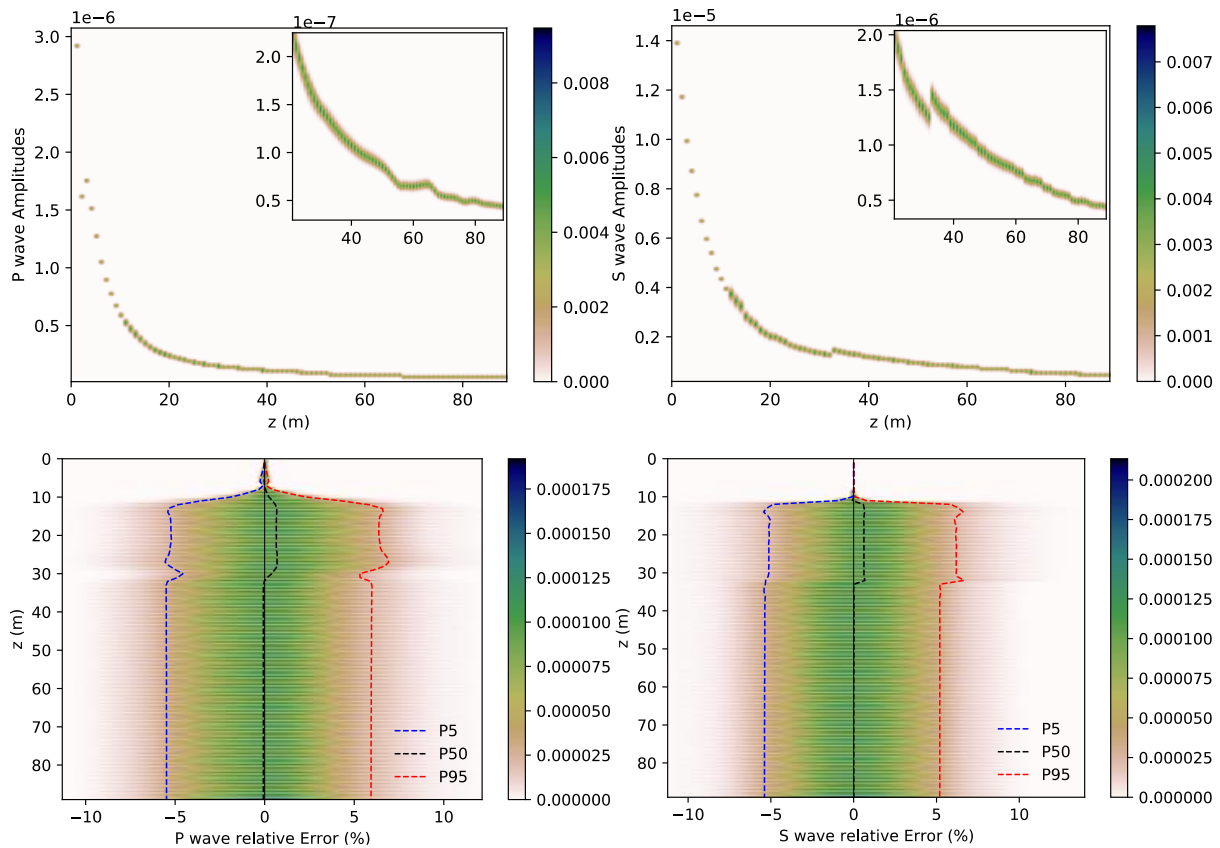


Figure 17: Probability density functions of correction terms and their associated errors as function of depth z for respectively P (leftmost) and S (rightmost). Zoom plots on P and S wave amplitude pdfs between $z = 21$ m and $z = 90$ m are shown on the upper right corners.

4.2.2. Density effect upon quality factor estimates

Like the case of the velocity, we investigate the impact of density error on the robustness of the proposed methods. An array of similar tests was performed by considering the data of Model A and trying to correct them using terms calculated after perturbing the density model. Both the regression method and the least-squares inversion are tested.

-The regression method: we started by estimating the attenuation coefficients of each layer using a linear piecewise regression. These values served then to calculate the seismic quality of each layer. The true velocity averages of each layer are considered in this experiment (Table 1). We finally obtained a set of 1000 estimates of each layer quality factor which permits to plot the histogram of the different Q factor values (Figure 18 and Figure 19) and to fit the corresponding distributions. Moreover, the associated errors were calculated and their histograms and distributions are plotted in the same figures. For both P-and S-waves, we can observe that the Q factor distributions differ from one layer to another. For example, estimates for Layer 1 are almost unbiased but show relatively large variances. The absence of any bias here can be explained by the low correction term errors observed for this layer (Figure 17) whereas the variance values may be due to the lack of data corresponding to this layer (e.g. only 8 points for P waves). On the other hand, Layer 2 and especially Layer 3 show both biased estimates but with very low dispersions. The observed bias seems not related to the introduced density perturbations since the Q factor averages are close to estimates obtained with noise-free data. We can attribute this to the method itself and the used approximations. The small variances find its origin in the large number of data available for these layers. According to this analysis, the density seems to impact some local data and does not influence a lot the slopes used to infer the attenuation coefficient.

Segments of the curve of corrected data as function of distance from sources are simply translated up and down but keep the same slopes.

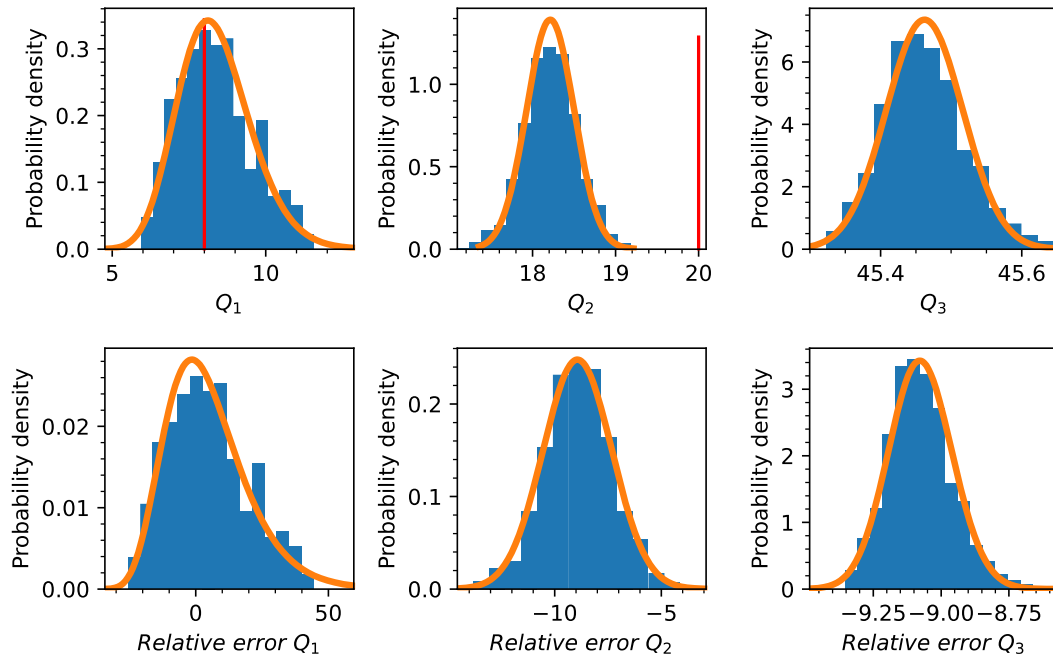


Figure 18: Distributions of P wave quality factors (upper 3 figures) and the associated relative errors (lower figures) for the 3 layers of Model A after perturbing their density values. Vertical red lines indicate the true quality factor of each layer (It is not shown for the last layer for visibility reasons).

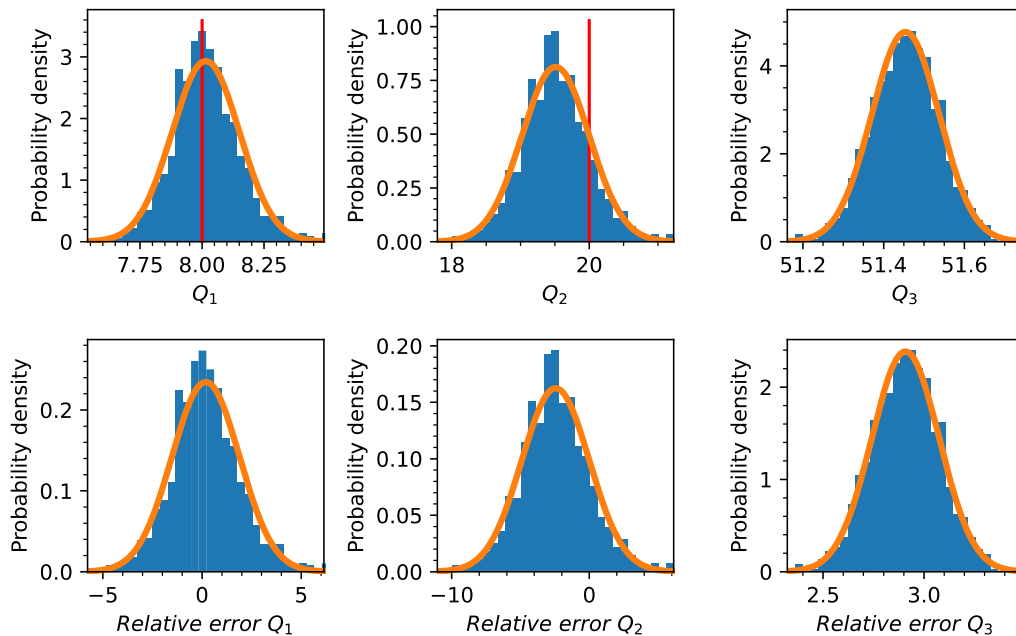


Figure 19: Distributions of S wave quality factors (upper 3 figures) and the associated relative errors (lower figures) for the 3 layers of Model A after perturbing their density values. Vertical red lines indicate the true quality factor of each layer but it is not shown for the last layer for visibility reasons.

- The least-squares inversion: the same test was also carried out with the inversion method. First, corrected data with the different terms were inverted to get the quality factor profiles. The three

Lagrangian constants ε , α and γ were respectively set to 1000, 1000 and 0.01. The set of these profiles were then used to generate the corresponding distributions (Figure 20). Obtained results of this experiment are very similar compared to those already found with the regression method. First, we noted low dispersion for the Q factor distribution of S waves as well as for the P wave estimates of the Layer 3. This may be explained by the quality and the number of data available for these layers. Besides, most of the layer quality factor estimates show slight biases but still very close to the noise-free data estimates. Except for Layer 1 and 2 where the density noises caused some perturbations of the P wave profiles, no effects are noted for Layer 3 and for all the estimates of S waves.

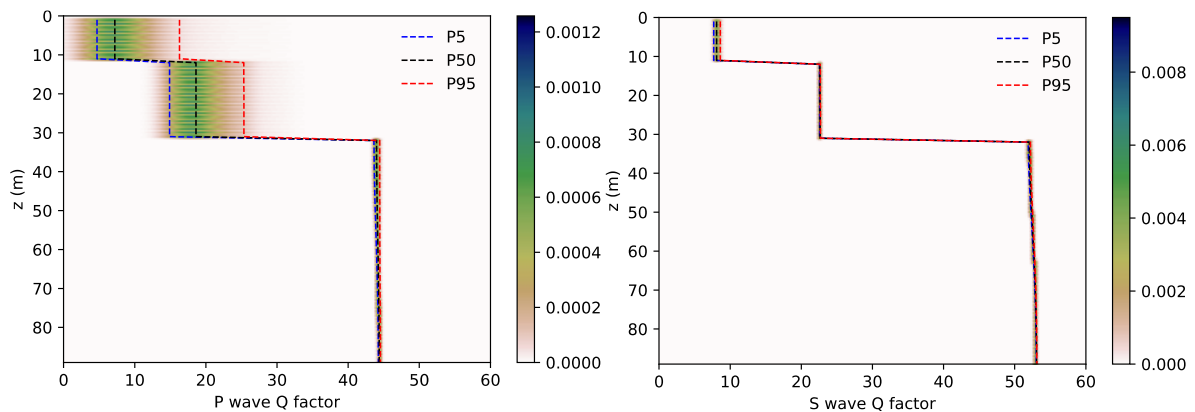


Figure 20: Probability density functions of P and S wave quality factors. The 5th (P5) and 95th (P95) percentiles as well as the median (P50) are calculated and plotted for each distribution.

5. Conclusion and outlooks

We proposed in this work a comprehensive approach to estimate the seismic quality factor using data measured in shallow boreholes in a downhole configuration. It includes a novel robust method to correct geometrical spreading as well as two techniques to determine a vertical profile of the quality factor for both P and S waves. The new geometrical spreading correction consists in scaling the seismic amplitudes picked on real seismograms using terms obtained after numerical modeling. More specifically, these correction terms are computed using the picked amplitudes of synthetic seismograms prepared using an elastic modeling that reproduces faithfully the acquisition conditions of the data, such as the subsurface structure, the velocity model, the source position and mechanism, and the receiver configuration. This approach was tested on two synthetic examples involving P and S waves and seems to properly compensate the geometrical spreading attenuation. Compared to existing methods, this correction can theoretically operate for complex geological structures and under different acquisition configurations. Besides accounting for geometrical spreading, the proposed technique also allows to automatically correct the source radiation pattern effect on the picked amplitudes, as long as the source is faithfully represented in the simulation.

The amplitudes obtained after applying the described correction are then analyzed to quantify the seismic attenuation. The first method is based on a piecewise linear regression of line segments constituting the curve of the corrected amplitudes plotted against source distances. This was made possible by demonstrating that for a downhole configuration and under the assumption of straight seismic ray paths and layered structure, seismic amplitude reduction is directly proportional to the attenuation coefficient of each layer. The method was tested on synthetic data and showed relative errors between 3% and 13%. We also noted that S wave data are in general easier to analyze than the P waves. This is due to the fact that P wave amplitudes cannot be reliably picked for the first receivers near the source because of its small amplitudes (due to the source radiation pattern) and the strong

interferences with S waves. It is important to note that high velocity variations within layers may also affect the robustness of this method by violating the linear aspect of the amplitude curves.

The second method is based on inversion of the seismic amplitudes. The analysis made in this paper showed that the amplitude corrected for geometrical spreading can describe a linear inversion problem that can be parameterized using either the attenuation coefficient (α) or the dissipation factor ($1/Q$). Three constraints were implemented to ensure stable solutions: 1- a second order Tikhonov regularization to smooth the recovered models, 2- an average constraint to impose mean values for chosen geological layers and 3- an equality constraint to reproduce the local known model parameters. The solution to this inversion problem is given by the least-squares method. A set of numerical experiments using synthetic data was carried out to test the method performance. After properly setting the Lagrange multipliers, the method allowed to approximately reproduce the true Q factor profiles. Note that generally the recovered models are widely controlled by the imposed Lagrange multipliers. These parameters must therefore be carefully chosen.

Finally, a stochastic analysis was performed to test the robustness of the proposed geometrical spreading correction against data noises. Throughout a bunch of tests, the presented correction method was proven to be very stable when perturbing the velocity or the density model. The same analysis also confirmed that S wave attenuation is easier and more reliable to estimate than P wave with either the inversion method or the piecewise regression. Finally, slight biases were sometimes observed for some seismic attenuation estimates. However, these biases seem to be more related to the different approximations than to the added noises.

Although the proposed methodology was shown to operate well in general, future work is planned to enhance some details and to fix secondary issues. For instance, it is mandatory to evaluate the performance of the proposed methods on real data. It would be better to perform several tests on many data sets with different acquisition modes adapted to P and S wave investigation. The step will be soon tackled. Unfortunately, data measured in a downhole configuration were acquired only at a single site at the time of this writing. It is therefore needed to schedule more acquisition campaigns. In particular, it is recommended to test acquisitions with several offsets and many active receivers per shot. Until new data are available, it is worthwhile to quantify the effects of factors impacting the approach performance. For instance, we have seen that sharp velocity variations may induce strong reflections that can create local amplitude variations (positive or negative depending on the type of interference between the direct and reflected waves). These variations can therefore affect the measured amplitudes as well as the modelled amplitudes used for the geometrical spreading correction. Adding a term to take into consideration reflection effects on measured and correction data seems to make the proposed correction more robust (Reine et al., 2012). Briefly, a general assessment of reflection effects is desirable. Finally, another possible improvement consists in testing other types of inversion criteria to estimate the Q factor profiles. In particular, the blocky inversion method may be an interesting alternative, as it is based on the minimization of the l-1 norm of the data misfit and it promotes piecewise constant models. This may better quantify the seismic attenuation.

6. References

- Aki, K., and B. Chouet, 1975, Origin of coda waves: source, attenuation, and scattering effects: *Journal of geophysical research*, **80**, no. 23, 3322-3342.
- Cervený, V., 2001, *Seismic ray theory*. Vol. 110: Cambridge university press Cambridge.
- Dasgupta, R., and R. A. Clark, 1998, Estimation of Q from surface seismic reflection data: *Geophysics*, **63**, no. 6, 2120-2128.
- Fabien-Ouellet, G., E. Gloaguen, and B. Giroux, 2017, Time-domain seismic modeling in viscoelastic media for full waveform inversion on heterogeneous computing platforms with OpenCL: *Computers & Geosciences*, **100**, 142-155.

- Frankel, A., and R. W. Clayton, 1986, Finite difference simulations of seismic scattering: Implications for the propagation of short-period seismic waves in the crust and models of crustal heterogeneity: *Journal of Geophysical Research: Solid Earth*, **91**, no. B6, 6465-6489.
- Giroux, B., M. Chouteau, and L. Laverdure, 2001, Évaluation du facteur de qualité sismique au barrage de Carillon (Québec): *Canadian Journal of Civil Engineering*, **28**, no. 3, 496-508.
- Li, G., M. D. Sacchi, and H. Zheng, 2016, In situ evidence for frequency dependence of near-surface Q: *Geophysical Journal International*, **204**, no. 2, 1308-1315.
- Mackie, R., and W. Rodi. 2010, Geophysical Inversion for Non-smooth Models. Paper read at Progress In Electromagnetics Research Symposium Abstracts, at Cambridge, USA.
- Mangriotis, M.-D., 2009, Scattering Versus Intrinsic Attenuation in the Near Surface: Measurements from Permanent Down-hole Geophones, UC Berkeley.
- Mangriotis, M.-D., J. W. Rector III, E. F. Herkenhoff, and J. C. Neu, 2013, Scattering versus intrinsic attenuation in the vadose zone: A VSP experiment: *Geophysics*, **78**, no. 2, B49-B63.
- Mari, J.-L., and C. Vergnialt, 2021, Well seismic surveying and acoustic logging: EDP Sciences.
- Newton, C., and R. Snieder, 2012, Estimating intrinsic attenuation of a building using deconvolution interferometry and time reversal: *Bulletin of the Seismological Society of America*, **102**, no. 5, 2200-2208.
- Padhy, S., and N. Subhadra, 2013, Separation of intrinsic and scattering seismic wave attenuation in Northeast India: *Geophysical Journal International*, **195**, no. 3, 1892-1903.
- Quan, Y., and J. M. Harris, 1997, Seismic attenuation tomography using the frequency shift method: *Geophysics*, **62**, no. 3, 895-905.
- Reine, C., M. van der Baan, and R. Clark, 2009, The robustness of seismic attenuation measurements using fixed-and variable-window time-frequency transforms: *Geophysics*, **74**, no. 2, WA123-WA135.
- Reine, C., R. Clark, and M. van der Baan, 2012, Robust prestack Q-determination using surface seismic data: Part 1—Method and synthetic examples: *Geophysics*, **77**, no. 1, R45-R56.
- Sedaghati, F., and S. Pezeshk, 2016, Estimation of the coda-wave attenuation and geometrical spreading in the New Madrid seismic zone: *Bulletin of the Seismological Society of America*, **106**, no. 4, 1482-1498.
- Sheriff, R. E., 2002, *Encyclopedic dictionary of applied geophysics*: Society of exploration geophysicists.
- Tonn, R., 1991, The Determination of the seismic quality factor Q from VSP data: a comparison of different computational methods: *Geophysical Prospecting*, **39**, no. 1, 1-27.
- Ursin, B., and K. Hokstad, 2003, Geometrical spreading in a layered transversely isotropic medium with vertical symmetry axis: *Geophysics*, **68**, no. 6, 2082-2091.
- Wang, C., J. Pei, and J. Wang. 2013, Near-surface Q model building and inverse Q filtering: A case study from Daqing oilfield, China. Paper read at 2013 SEG Annual Meeting.
- Xu, S., and A. Stovas, 2017, Three-dimensional generalized non-hyperbolic approximation for relative geometrical spreading: *Geophysical Journal International*, **211**, no. 2, 1140-1153.